

CIS Photovoltaic Technology

Final Technical Report

12 January 1997 - 15 April 1998

A.E. Delahoy, J.S. Britt, and Z.J. Kiss
Energy Photovoltaics, Inc.
Lawrenceville, New Jersey



National Renewable Energy Laboratory
1617 Cole Boulevard
Golden, Colorado 80401-3393
A national laboratory of the U.S. Department of Energy
Managed by Midwest Research Institute
for the U.S. Department of Energy
under contract No. DE-AC36-83CH10093

CIS Photovoltaic Technology

Final Technical Report

12 January 1997 - 15 April 1998

A.E. Delahoy, J.S. Britt, and Z.J. Kiss
Energy Photovoltaics, Inc.
Lawrenceville, New Jersey

NREL technical monitor: H.S. Ullal



National Renewable Energy Laboratory
1617 Cole Boulevard
Golden, Colorado 80401-3393
A national laboratory of the U.S. Department of Energy
Managed by Midwest Research Institute
for the U.S. Department of Energy
under contract No. DE-AC36-83CH10093

Prepared under Subcontract No. ZAF-5-14142-04

October 1998

This publication was reproduced from the best available copy
Submitted by the subcontractor and received no editorial review at NREL

NOTICE

This report was prepared as an account of work sponsored by an agency of the United States government. Neither the United States government nor any agency thereof, nor any of their employees, makes any warranty, express or implied, or assumes any legal liability or responsibility for the accuracy, completeness, or usefulness of any information, apparatus, product, or process disclosed, or represents that its use would not infringe privately owned rights. Reference herein to any specific commercial product, process, or service by trade name, trademark, manufacturer, or otherwise does not necessarily constitute or imply its endorsement, recommendation, or favoring by the United States government or any agency thereof. The views and opinions of authors expressed herein do not necessarily state or reflect those of the United States government or any agency thereof.

Available to DOE and DOE contractors from:
Office of Scientific and Technical Information (OSTI)
P.O. Box 62
Oak Ridge, TN 37831
Prices available by calling (423) 576-8401

Available to the public from:
National Technical Information Service (NTIS)
U.S. Department of Commerce
5285 Port Royal Road
Springfield, VA 22161
(703) 605-6000 or (800) 553-6847
or
DOE Information Bridge
<http://www.doe.gov/bridge/home.html>



Preface

This report describes work performed during the third phase (January 12, 1997 - April 15, 1998) of a three-phase, cost-shared subcontract with NREL entitled "CIS Photovoltaic Technology". The subcontract is one component of the **NREL Thin Film Partnership Program**. Remarkably high conversion efficiencies (15 - 17.6%) have been demonstrated for small area Cu(In,Ga)Se₂ devices in the U.S., Europe, and Japan. A major objective of this subcontract has been to demonstrate the preparation of high quality CIGS material over large areas (0.43 m²) using novel equipment and processes that are adaptable to high throughput manufacturing. Using this material, glass-glass laminated CIGS PV modules have been produced in a pilot line. Research results generated by other components of the Thin Film Partnership Program and working groups have been incorporated as needed.

Needless to say, the results described here could not have been achieved without the diligent efforts of the EPV research, engineering and support staff. Other institutions and individuals have also contributed significantly. At NREL we would like to thank S. Asher, H. Field, A. Franz, R. Matson, A. Mason, and A. Swartzlander for invaluable material and device characterization, T. Coutts, T. McMahon, and J. Tuttle for helpful technical discussions, and especially R. Noufi for his consistent help to industry to advance CIGS technology. On the program side, we are indebted to H. Ullal and K. Zweibel for their unflagging interest and support. We have benefited also through interaction with the Institute of Energy Conversion/University of Delaware, and through participation in the substrate/Mo/Na working group in collaboration with Colorado State University, the University of Illinois, International Solar Electric Technology, and Lockheed Martin Astronautics.

Summary

Energy Photovoltaics, Inc. has explored novel sequential formation recipes for CIGS that can be implemented on a unique pilot line constructed to coat low cost, glass substrates 4300 cm² in area. One particular feature of this line is the use of proprietary linear sources capable of downwards evaporation.

Implementation of a particular CIGS recipe on the pilot line enabled large area modules to be prepared with efficiencies up to 7.6%. In this recipe, In_xGa_ySe_z is formed on the substrate, followed by metal deposition to supply the Cu, and the resulting precursor is selenized and terminated with additional In and Ga.

Electrical resistance monitoring of the film was shown capable of indicating the temperature of compound formation and detecting termination. Both IGS and CIGS films were analyzed by X-ray diffraction; no binary phases were detected in the CIGS, while peaks attributed to CIGS and CGS were observed, as well as CIS. The diffusion and reaction of Ga was studied by deposition of Ga at different temperatures onto Ga-free precursors followed by selenization and Auger depth profiling.

The substrate/Mo/Na working group (EPV, ISET, LMA, UI, CSU, NREL) studied Na in Mo, and the effect of Na on devices, finding it beneficial except at concentrations exceeding 0.4%. SIMS profiles suggested segregation of Na towards the Mo interface.

Properties of large area, magnetron sputtered ZnO:Al were: sheet resistance 24 Ω/sq., transmission 82%, conductivity 440 S cm⁻¹. Preheating of the glass was found to increase the conductivity.

Devices prepared using a baseline CIGS process averaged 11.7% in efficiency. Considerable efforts were expended studying dark aging effects, light-induced recovery, and cyclic effects in devices utilizing this process, and the effect of moisture on CIGS prior to device fabrication. Later it was discovered that a new CIGS process developed at EPV yielded devices that did not suffer from dark aging effects. This promising process was termed the FORNAX process. It remains to be implemented on the pilot line.

Modules and minimodules were prepared using a diode-laser-pumped YAG laser for the Mo patterning, and mechanical scribing for the subsequent cuts. A 9.7% minimodule was demonstrated.

Large area CIGS formation involves the use of linear sources, and thickness profiles were presented for simple and optimized linear sources. An unencapsulated module producing 25 watts (7.65% aperture area efficiency) was produced.

Using a new diagnostic technique, the fill factor of a CIGS module was decomposed into contributions from the intrinsic device fill factor and ZnO sheet resistance.

Table of Contents

Preface	. i
Summary	. ii
Table of Contents	. iii
List of Figures	. iv
List of Tables	. v
Introduction	. 1
1.0 CIGS Deposition and Analysis	. 2
1.1 Review of General Principles for forming Device-quality CIS or CIGS films	. 2
1.2 Review of General Categories of Absorber Processes	. 3
1.3 Absorber Formation	. 4
1.31 Review of EPV's CIGS formation processes	. 4
1.32 Resistance monitoring	. 5
1.33 Effect of the evolution of compound source material	. 6
1.4 Structure, Composition and Profiling	. 7
1.41 XRD of CIGS films	. 7
1.42 Ga composition profiles.	. 9
1.5 Findings of the Substrate/Mo/Na Working Group	. 10
2.0 Zinc Oxide	. 12
2.1 Deposition and Properties	. 12
2.2 Doping and Impurities	. 13
2.3 Substrate Heating.	. 13
3.0 Device Studies	. 14
3.1 Baseline Process	. 14
3.2 Aging and Light-soaking Effects	. 14
3.21 Dark aging	. 14
3.22 Recovery via light soaking	. 16
3.23 Cyclic dark aging/light soaking	. 19
3.24 Effect of moisture after CIGS formation	. 20
3.25 Stability of CIGS prepared by new FORNAX process	. 21
4.0 Minimodule Fabrication	. 22
4.1 Purpose and Methods	. 22
4.2 Results	. 22
5.0 Module Fabrication and Performance	. 23
5.1 Processing Steps	. 23
5.2 Linear Source Evaporation	. 24
5.3 Patterning.	. 24
5.4 Encapssulation	. 25
5.5 Module Performance	. 27
5.6 Module Diagnostics	. 28
References	. 29

List of Figures

- 1.1. Sheet resistance during the formation of CIGS films with and without a termination step.
- 1.2. Auger depth profiles of Ga/(Ga+In) in CIGS films with identical amounts of Ga deposited at various substrate temperatures.
- 1.3. SIMS profile for EPV CIGS on Mo-coated soda-lime glass.
- 2.1. ZnO film characteristics before and after changing the Ar cylinder
- 3.1. Effect of aging on average device efficiency for selenized CIGS films
- 3.2. Device degradation after 75 days storage as a function of the initial V_{oc} x FF.
- 3.3. Average efficiency of runs after 1 hr. light-soaking vs. the average efficiency prior to light-soaking, both normalized to the initial efficiency.
- 3.4. J-V characteristics as a function of light-soaking time.
- 3.5. Experimental diode quality factor and series resistance as a function of light-soaking time.
- 3.6. The improvement of devices upon light-soaking as a function of their V_{oc} , FF product prior to light-soaking.
- 3.7. The improvement of devices upon 1 hr. light-soaking as a function of the amount of degradation in the V_{oc} , FF product after 75 days.
- 3.8. Normalized efficiency of devices from H1725 over the course of time.
- 3.9. Effect of CIGS storage under various conditions prior to CdS/ZnO deposition.
- 3.10. Change in V_{oc} x FF for three sets of FORNAX devices as a function of time.
Devices were stored in lab ambient between measurements.
- 4.1. I-V curves of a set of minimodules from run 1724.
- 5.1. Thickness profiles obtained for simple and optimized linear evaporation sources
- 5.2. Monolithically integrated CIGS module showing interconnect scheme and metal foil busbars at module edges.
- 5.3. Layout of CIGS plate prior to lamination.
- 5.4. I-V curve measured by NREL for a 19.7 watt, 3156 cm² glass-glass gure encapsulated CIGS module.
- 5.5. I-V curve measured in sunlight at EPV for a 25 watt, 7.65% CIGS module.

List of Tables

- 1.1. Effect of the termination step on device characteristics as a function of the fraction of source material remaining.
- 1.2. InGaSe phases observed by XRD.
- 1.3. CIGS phases observed by XRD.
- 1.4. EPMA (20kV) of CIGS films with identical amounts of Ga deposited at various substrate temperatures.
- 1.5. Effect of sodium on CIGS device performance
- 2.1. Properties of ZnO prepared on unheated and pre-heated glass
- 3.1. Average device characteristics for the baseline selenization process.
- 3.2. Ratios of V_{oc} , FF, and $V_{oc} \times FF$ after 1 hr. light-soaking at AM1.5 relative to their initial values.
- 3.3. Device parameters as a function of light-soaking time.
- 4.1. Photovoltaic parameters of the set of minimodules.
- 5.1 Quality Control Procedures for CIGS Module Fabrication
- 5.2. Comparison of predicted module fill factor (based on diagnostic data) and measured module fill factor for seven CIGS modules

Introduction

Thin film photovoltaic modules based on Cu(In,Ga)Se_2 have been shown to possess attributes that should enable them to compete effectively with silicon-based modules, and that should ultimately allow realization of a lower $\$/W_p$ cost figure. These attributes are stability, high efficiency, and low materials cost. In addition,

The following guiding principles have been observed by Energy Photovoltaics, Inc. in its development of CIS and CIGS technology. Firstly, for safety reasons, solid elemental selenium is used, and not hydrogen selenide; secondly, an all-vacuum process is used to ensure even, defect-free coating and impurity control; thirdly, scalable deposition methods are used (and where needed, developed); and lastly, the substrate is glass, the flattest, lowest cost substrate available offering structural support and high temperature capability.

1.0 CIGS Deposition and Analysis

1.1 Review of General Principles for Forming Device-Quality CIS or CIGS Films

We present below guidelines for producing device-quality CIGS. This review was previously presented by EPV in [1].

Adhesion

- For Mo, utilize a bilayer structure (thin, high ρ , highly adherent layer grown at high pressure, followed by thicker, low ρ layer at low press.)
- For CIGS, provide a suitable adhesion layer, by accident or design

Sodium

- Arrange for adequate Na source (soda lime glass or extrinsic source, Mo type and [O])

Cu-rich matrix

- Provide a Cu-rich precursor (or CIS + Cu_xSe) with $\text{Cu}/\text{In} > 1$
- Cu_xSe phase melts at $T = 525\text{ }^\circ\text{C}$, offering possibility of recrystallization
- Supply In, (Ga), and Se to convert Cu_xSe to CIS (CIGS), preferably at $T = 550\text{ }^\circ\text{C}$, to provide an In-rich surface layer (termination), and to arrive at a global composition $0.86 < \text{Cu}/(\text{In}+\text{Ga}) < 0.96$.

Se overpressure

- Form stable binary and ternary phases during *growth*, not termination
- Use Se/metal flux ratios of 3 for Cu-Se binaries or ternaries, 5 for (In,Ga)-Se binaries
- Thus $\text{In}_2\text{Se} + \text{Se} \rightarrow \text{InSe}$ or In_2Se_3 inhibiting In loss via In_2Se desorption

In-Ga profile and bandgap grading

- CIS on CGS (CuGaSe_2) is superior to CIS only, presumably because of a back-surface field; if Ga in precursor only, it segregates at back. Best devices are CIGS absorber on CGS; Ga supplied at high temp.
- Termination processes (e.g. in 3-stage recipes) result in a desirable notch structure (or double conduction bandedge grading)

Built-in shallow n-p junction

- Promote surface 1:3:5 composition n-OVC layer (bulk CIS is p-type); see also *buffer layer*

Buffer layer (e.g. CBD CdS)

- a physical barrier layer to limit sputter damage
- other possible roles are to enhance character of OVC, dope surface n-type by Cd incorporation, change conductivity of bulk

Compatible transparent conductor

- ZnO (0.05 μm i-ZnO + 0.5 μm -ZnO:Al) + optional AR coating

1.2 Review of General Categories of Absorber Formation Processes (for CIS and CIGS)

This section reviews and describes the main categories of absorber formation recipes appearing in the literature. The review was originally presented in [1].

(1) One-stage (coevaporation of all elements at all times)

variations: constant or variable rates (Boeing bilayer; in-line processing)

- at 450 C, Cu + In + Ga + Se \rightarrow CIGS/Cu_xSe
- at 550 C, with Cu flux \downarrow CIGS/Cu_xSe + Cu + In + Ga + Se \rightarrow CIGS
In \uparrow , Ga \downarrow = normal grading
ditto, then inverse = double grading

cool to 350 C in 20 min. in Se.

(2) Two-stage (coevaporation/termination)

- at 500 C, Cu + In + Ga + Se \rightarrow CIGS/Cu_xSe
- at 550 C, CIGS/Cu_xSe + In + Ga + Se \rightarrow CIGS (no Cu in 2nd stage) overall time 30 min.

(3) Three-stage (sequential delivery of metals with Se/termination)

- at 260 - 300 C, In + Ga + Se \rightarrow (In,Ga)Se_x hexagonal
- at 550 C, (In,Ga)Se_x + Cu + Se \rightarrow CIGS/Cu_xSe (Se prevents In loss)
- at 550 C, CIGS/Cu_xSe + In + Ga + Se \rightarrow CIGS (10-15% In,Ga added) overall time 50 min., typically 2.7 μm film, cool to 350 C in 20 min. in Se

Simplifies in situ process control

Radius of In atom < Ga; strain lowered by outdiffusion of In leaving Ga at back. Ga placed at surface in termination step.

(4) Selenization (sequential delivery of metals without Se/compound formation in Se vapor)

- at low T, (Cu,In) + (Cu,Ga) \rightarrow Cu_xIn + Cu_yGa + Cu + In
- + Se during temperature ramp \rightarrow Cu_xSe + (In,Ga)_ySe
- at 450 C, + Se \rightarrow CIGS

Separates deposition processes from thermal/chemical processes

Either H₂Se or elemental Se vapor is used

Complex reactions

(5) Sequential process with compound source (Se-containing precursor/selenization)

- at low T, precursor formation
- at high T, compound formation

Examples:

- 200 C, evaporated InSe_x (amorphous) + Cu
- selenize \rightarrow CIS (bilayer)

- Cu + InSe_x
- selenize \rightarrow CIS (poor adhesion)

Cu front moves through film, Cu_xSe promotes recrystallization
Use few nm of GaSe_x to promote adhesion

- (thin adhesion layer) + Cu + InSe_x + $\text{GaSe}_x \rightarrow$ CIGS (by XRD)
- GaSe_x + Cu + $\text{InSe}_x \rightarrow$ CIS + CIGS (by XRD)

(6) Sequential process with compound source and termination

(7) Stacked elemental layers with selenization

- at RT, metal stack + a-Se (30% excess)
- RTP to avoid dewetting of Se at 100 - 200 C; some In loss

At 300 C, Cu_4In InSe CuSe CIS
400 C, CuSe CIS
500 C, CIS
550 C, CIS CIGS

Na promotes presence of CuSe at higher temperatures

- **Other variable gap structures**
- at 500 C, Cu + Ga + Se \rightarrow CGS + Cu_xSe (CGS is small-grained)
- at 550 C, + In + Se \rightarrow CIGS (by XRD)
If Ga and In are interchanged, the product is CGS + CIS

1.3. Absorber Formation

1.3.1 Review of EPV's CIGS formation processes

Prior to the end of this subcontract, EPV progressed to the third of its absorber formation processes. The first process was vacuum selenization of metal precursors. The second process can be described as a sequential process with compound source and termination [2,3]. It is the process by which EPV's best large area modules have been made, and unless otherwise indicated, it is the subject of most of the work reported here. EPV's third

process has been designated the FURNAX process. It differs in the substrate temperature during Cu delivery (among other matters), and results in higher open-circuit voltages and superior cell stability.

1.32 Resistance monitoring

Differences in carrier concentration can be used to distinguish between Cu-rich and Cu-poor CIS films, thereby avoiding the continuous monitoring and rate integration of the evaporant fluxes with sophisticated instrumentation. Stoichiometric or Cu-poor CIS films have hole concentrations less than 10^{16} cm^{-3} , while the presence of the Cu_{2-x}Se phase in Cu-rich CIS films abruptly raises the hole concentration to $10^{19} - 10^{20} \text{ cm}^{-3}$ with profound effects on emissivity and electrical conductivity [4]. The former property has been exploited by Matsushita to develop a temperature monitoring technique to identify the compositional transition under conditions of constant thermal radiation [5]. In-situ conductivity measurements have been performed previously to study the reaction kinetics of CIS and CGS films deposited by a sequential process directly on glass [6]. We have investigated the continuous monitoring of the electrical conductivity during the deposition process for its utility in identifying the Cu-rich to Cu-poor transition.

Instead of a specially patterned Mo, the laser-scribed Mo typically employed for module fabrication was used as the back contact to the CIGS film. Precursors were deposited in the pilot line on the laser-scribed Mo. Electrical connection to the Mo was made at the sample ends with pressure point contacts. The total electrical resistance is then the sum of the resistances of the Mo film and the forming CIGS film across each laser scribe. The contribution to the total resistance from the glass was found to be less than 1% at all temperatures explored, although evidence for sodium ion migration in the glass was observed when alternating bias polarity, particularly at temperatures above 400°C . Because the sheet resistance of the Mo film is low ($\sim 2 \Omega/$), its contribution to the total electrical resistance could also be neglected under most conditions. Resistance was monitored directly in a two-wire configuration. An ohmic contact was verified after each experiment with a 10V IV measurement.

Two precursors were prepared, one designed to yield only slightly Cu-rich CIGS (A), the other more Cu-rich CIGS (B). Two adjacent samples from precursor A and one sample from precursor B were selenized independently from 225°C - 530°C under a continuous flux of Se. One of the samples from precursor A was terminated with 500 In while the substrate was at 530°C to convert it from Cu-rich to Cu-poor. After selenization, EPMA was performed at 20 kV on all three samples to determine Cu/(In+Ga). The sheet resistance of the three films, calculated from the scribe dimensions, and the substrate temperature profile are plotted in Figure 1.1 as a function of the selenization time.

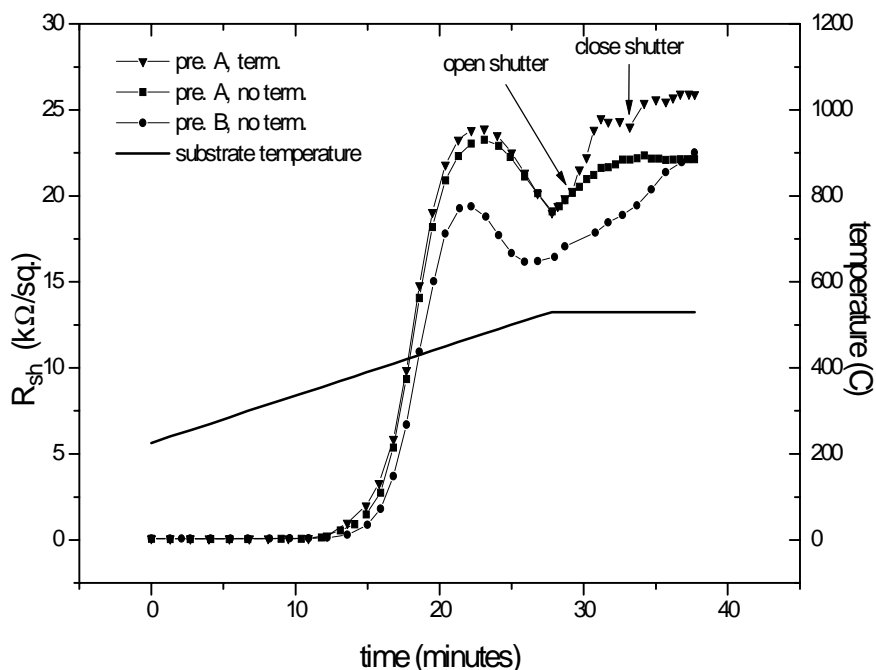


Figure 1.1. Sheet resistance during the formation of CIGS films with and without a termination step.

In all cases, there was little change in the sheet resistance up to a temperature of about 375°C at which point it increased rapidly until reaching a peak at about 475°C. This is consistent with reports that CIS forms by the two step process at about 450°C [7]. The sheet resistance of the CIGS made from the more Cu-rich precursor B ($\text{Cu}/(\text{In}+\text{Ga}) = 1.21$) was found to increase steadily during the soak at the terminal temperature of 530°C, while the sheet resistance of CIGS from precursor A (no termination, $\text{Cu}/(\text{In}+\text{Ga}) = 1.07$) reached an equilibrium after 5" at 530°C. This result may be explained by a more defective grain structure or grain boundaries in Cu-rich CIGS films. It is likely that phase segregation related to precursor preparation could lead to similar behavior in Cu-poor CIGS films.

Upon initiating the termination process for precursor A, the sheet resistance rose quickly and then stabilized before the In source was shuttered. After the shutter was closed, the sheet resistance re-stabilized at a value 1.2x that of the non-terminated film. After cooling to 475°C, the sheet resistance of the Cu-poor film was greater than 2x that of the Cu-rich film. Upon cooling to room temperature, the sheet resistances of the terminated (Cu-poor) and non-terminated (Cu-rich) CIGS films were 5.3×10^7 and $3.0 \times 10^4 \Omega/$, respectively. The terminated film was found to have $\text{Cu}/(\text{In}+\text{Ga}) = 0.91$. The relatively small difference in sheet resistance between Cu-rich and Cu-poor films at high temperature is evidence that the carrier concentrations are in the intrinsic range.

1.33 Effect of the evolution of compound source material on termination

A proprietary source material deposited by evaporation is used at EPV to form CIGS films. Evolution of the source material has been observed by Auger depth profiling of films deposited by completely evaporating a charge of the source onto cold substrates. The evolution occurs primarily during the deposition of the last 50% of the charge. The effect

of this evolution on device properties has been explored. A charge sufficient for several terminations was loaded into an evaporation boat. Approximately ½ the charge was evaporated off before starting this set of experiments. Thus, these experiments represent the last 50% of the source lifetime.

Identical precursor material was selenized and terminated in three successive depositions and the device properties of the resulting CIGS was evaluated. The termination step was conducted according to a recipe currently optimized for device efficiency. The best device characteristics from each deposition are listed in the table below. Evaluation of three devices on each sample show a small improvement in V_{oc} and a larger improvement in fill factor with successive depositions. It is encouraging that the magnitude of the improvement in efficiency is relatively small.

Table 1.1. *Effect of the termination step on device characteristics as a function of the fraction of source material remaining.*

sample #	source life %	V_{oc} mV	J_{sc} mA/cm ²	FF %	Eff. %
814B-3H3	33-50	510	34.5	64.5	11.3
814B-3H2	17-33	519	33.2	66.1	11.4
814B-3H1	0-17	519	35.0	69.6	12.6

1.4 Structure, Composition, and Profiling

1.41 XRD of InGaSe and CIGS films

Two InGaSe films on Mo were analyzed by XRD (see Table 1.2). The first one, 811B, was a film deposited in the pilot system. The nominal substrate temperature during deposition was 300°C. The second film, 860-1, was deposited in the R&D reactor at a substrate temperature of 300°C and is about 1200 Å thick. No additional Se was present during either deposition.

The concentration of In, Ga, and Se in these two films is given at the bottom of Table 1.2. The concentration of 860-1 had to be measured by XPS because of the thinness of the film. The ratio Ga/(Ga+In) as well as Se/(Ga+In+Se) is considerably higher for 811B than 860-1. The only significant peak in sample 811B is attributed to Ga₂Se₃ (200). Sample 860-1 is essentially amorphous. We believe film 811B can be explained by an evolution of the source towards more Ga- and Se-rich compounds as the more volatile Se-poor selenides of In and Ga (resp.) leave. Whether a base layer with these characteristics is necessary or desirable for reliable and efficient devices remains to be seen.

Table 1.2. InGaSe phases observed by XRD.

comp.	811B		860-1			
%	d	rel. int.	d	rel. int.	desig. mat.	desig. d
	4.1449	2	4.160	2	InSe (004)	4.1700
	3.1553	12	-	-	Ga ₂ Se ₃ (200)	3.1500
	2.2265	100	2.2276	100	Mo (110)	2.2247
	1.2962	2	1.2947	2	-	-
	1.2856	2	1.2865	2	Mo (211)	1.2847
	1.2811	2	1.2835	2	-	-
	1.2729	2	1.2796	2	-	-
	1.1135	4	1.1135	4	Mo (220)	1.1129
	1.1105	4	1.1057	2	-	-
In	17.6	EPMA	33.2	XPS		
Ga	26.1	EPMA	27.1	XPS		
Se	56.3	EPMA	39.7	XPS		

Two CIGS films were submitted for XRD analysis (see Table 1.3 below). The first one, 740B2, was formed entirely within the pilot line and was cut from the module submitted to NREL before encapsulation. This plate had a thin termination with InGaSe (approximately 5% of the total In+Ga). The second sample 743b-1r1, was a pilot line precursor cut up and selenized in the R&D reactor with no terminating step. Also included in Table 1.3 is XRD data from a CIS film (no Ga) selenized in the R&D reactor (H1a) that was taken several years ago.

Table 1.3. CIGS phases observed by XRD.

740B2		743b-1r1		H1a			
d	rel. int.	d	rel. int.	d	rel. int.	desig. mat.	desig. d
present	-	5.1811	4	5.1945	2	CIS (101)	5.1700
3.3385	100	3.3434	100	3.3491	100	CIS (112)	3.3510
3.2501	20	3.2454	15	-	-	CuIn _{0.3} Ga _{0.7} Se ₂ (112)	3.2500
3.2224	15	-	-	3.2227	3	CIS (111)	3.2200
present	-	2.5225	4	2.5268	2	CIS (211)	2.5280
2.2308	250	2.2318	104	2.2328	20	Mo (110)	2.2247
2.0456	45	2.0465	31	2.0496	16	CIS (220)	2.0460
1.9880	7	1.9870	5	-	-	CGS (220)	1.9870
1.7453	20	1.7459	13	1.7467	8	CIS (312)	1.7450
1.7264	8	1.7233	4	-	-	CuIn _{0.7} Ga _{0.3} Se ₂ (312)	1.7280
1.4487	5	present	-	1.4469	2	CIS (400)	1.4460
1.3278	5	1.3278	4	1.3296	3	CIS (332)	1.3250
1.2880	5	1.2874	4	-	-	Mo (211)	1.2847
1.1824	5	1.1815	4	1.1842	2	CIS (424)	1.1820
1.1151	15	1.1159	6	-		CIS (512)	1.1130
-	-	1.1123	4	1.1144	2	Mo (220)	1.1129

The first observation is that all the films have a preferred (112) orientation. The sample made entirely within the pilot line is less oriented than the sample selenized in the R&D reactor. Neither of these first two Ga-containing samples have as strong a preferred orientation as the CIS film. No discernible peaks were found that can be attributed to binary phases in any of the films. There are three peaks of significant amplitude found in the two films with Ga that are not found in the Ga-free CIS film. The three peaks can be attributed to phases of CIGS and CGS. The strongest CGS peak (112. d-3.2100) was not found but may be buried within the CIS (111) peak at d-3.2200. The CGS (220) peak at d-1.9870 was identified. The peak attributed to $\text{CuIn}_{0.7}\text{Ga}_{0.3}\text{Se}_2$ (312) was identified directly from the JCPDS-ICDD file for that compound. The d- value for $\text{CuIn}_{0.3}\text{Ga}_{0.7}\text{Se}_2$ was identified by interpolating between experimental data taken from bulk CIGS samples. The presence of a number of phases with various Ga concentrations is not surprising, given the large gradients of Ga through these films as detected by Auger. What is surprising is that any phase exists with a high enough concentration to be identified as a single peak, instead of appearing as a broad peak with small amplitude, a result of “smearing”.

1.42 Ga composition profiles

It is generally difficult to incorporate an appreciable amount of Ga in the active region of a CIGS film formed by the simple selenization of metallic precursors. Regardless of its location in the precursor stack, Ga has been observed to segregate to the back of the film and the resulting film is phase-separated with CGS near the Mo electrode and CIS at the film surface for $\text{Ga}/(\text{Ga}+\text{In}) < 0.6$ [8]. This segregation has been thought to occur because of the lower temperatures required to form CIS compared to CGS. An experiment was conducted to test this hypothesis.

A Ga-free precursor was prepared by evaporating 300 In_2Se_3 onto a 1 ft² Mo-coated substrate, followed by the sequential evaporation of Cu and In, such that the Cu/In in the precursor was about 1.20. In_2Se_3 was used to improve the adhesion of the CIS film to the Mo. The plate was cut into smaller sections and the individual pieces were selenized from 180°-520°C and in three separate experiments identical amounts of elemental Ga were evaporated (3 /sec.) while soaking at different temperatures. The amount of Ga evaporated was chosen to make the final film slightly Cu-poor. The three soak temperatures examined were 250°, 375°, and 425°C. After selenization, a section from each CIGS film was submitted for EPMA and Auger depth analysis. The sample that had Ga deposited at 250°C had poor adhesion as determined by tape test while the other two samples had good adhesion.

The EPMA done at 20kV for each of the samples is shown in Table 1.4. The ratios of $\text{Ga}/(\text{Ga}+\text{In})$ as calculated from the Auger data is shown in Figure 1.2. Based on the Auger data, the EPMA samples the atomic constituents at about 0.6 μm from the surface. The Ga profile in the sample with Ga deposited at 250°C has a gaussian profile centered in the middle of the film, while the profiles of the films with Ga deposited at 375° and 425°C show the Ga is found primarily at the film surfaces with the concentration decreasing rapidly away from the surface. This implies that the Ga stops diffusing to the back (or In to the surface) long before the film reaches 450°C.

Table 1.4. EPMA (20kV) of CIGS films with identical amounts of Ga deposited at various substrate temperatures.

Ga dep. temp.	Cu	In	Ga	Se	Ga/(Ga+In)
250° C	22.0	22.5	4.3	51.1	0.161
375° C	21.9	16.7	10.2	51.2	0.308
425° C	21.5	17.4	9.7	51.4	0.358

According to the standard growth model, CIS forms only at temperatures above 450°C. Thus, it appears that Ga diffuses to the Mo not during the formation of CIS, but probably during the reaction of In with Se to form In_xSe_y compounds, which occurs at a lower temperature than the formation of Ga_xSe_y compounds. This suggests that precursors with well-mixed selenides of In and Ga could yield CIGS films with only small gradients in $Ga/(Ga+In)$. These conclusions are supported by earlier deposition experiments where InGaSe/Cu precursors were selenized and made into devices with open-circuit voltages over 600mV.

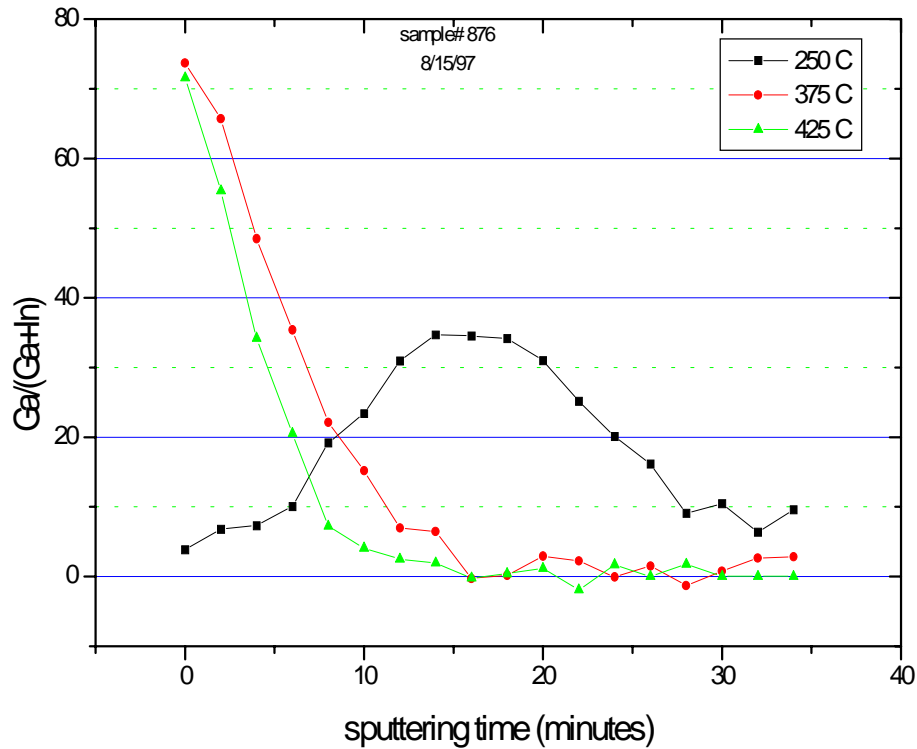


Figure 1.2. Auger depth profiles of $Ga/(Ga+In)$ in CIGS films with identical amounts of Ga deposited at various substrate temperatures.

1.5 Findings of the Substrate/Mo/Na Working Group

The effect of sodium on device performance was studied using both Na-free glass and soda lime glass and various levels of intentionally added Na. Thus borosilicate glass (7059, Lockheed Martin) was run side by side with soda lime glass (EPV) during precursor deposition and selenization with elemental Se at EPV. Sodium was incorporated into the

films by evaporation of Na₂S, the atomic % being estimated from the mass evaporated. Devices were fabricated and characterized at EPV, and the films were analyzed by EPMA (A. Swartzlander), SEM (R. Matson), SIMS (A. Rockett), and GIXRD (J. Ryker).

CIGS films on 7059 glass with no extrinsic Na appeared to be small-grained and buckled, with large gaps between the Mo and CIGS. The addition of Na, up to a concentration of 0.4%, led to significantly larger grains and less delamination. At 3% Na, the crystallinity had degraded, the film was small-grained, and delamination was observed.

Device results are summarized in Table 1.5 below. For devices on 7059 glass the fill factor increased with increasing Na up to 0.4%, while V_{oc} only improved at 3% Na. For devices on soda lime glass, the low-Na efficiency was higher, and the efficiency declined steadily with increasing Na.

Table 1.5. *Effect of sodium on CIGS device performance*

Sample	Cu/(In+Ga)	Na (atom. %)	V _{oc} (mV)	J _{sc} (mA/cm ²)	FF (%)	Eff. (%)
MM6b1	0.88	0	396	35.8	57.9	8.2
MM1a2/EPV2b	0.90/0.89	0.06	404/475	39.1/39.6	65.1/70.5	10.3/13.2
MM2a1/EPV3a	0.88/0.88	0.4	398/433	32.7/35.1	67.7/67.4	8.8/10.2
MM2a2/EPV2a	0.92/0.90	3.0	454/350	33.1/34.1	57.4/49.3	8.6/5.9

Work elsewhere has shown that Na is easily incorporated at the grain boundaries of sputtered Mo films, while in CIS, Na decreases the activation energy for electrical conductivity. SIMS analysis (University of Illinois) of Mo sputtered by EPV, ISET, and LMA revealed significant quantities of Na and O, with Na/O relatively constant within each film. The source of the O is believed to be residual gas in the sputtering system. Annealed (450 °C, 20 mins) Mo/glass substrates yielded ten times more Na. Attempted selenization of Mo on glass yielded significant selenization depths with H₂Se and little selenization with elemental Se. After H₂Se selenization an increase in Na similar to that resulting from annealing was found.

To study Na in CIS, CIS was coated on Mo/Sglass at EPV and ISET. The EPV samples exhibited almost an order of magnitude less Na near the outer surface, enhanced Na near the Mo interface, and a larger sample-to-sample variation. Possible explanations are different selenization chemistry, or thermal exposure. A typical SIMS profile of EPV CIGS on Mo-coated soda-lime glass is shown in Figure 1.3. The profiles are consistent with segregation of Na toward the Mo interface, perhaps controlled by CIS microstructure.

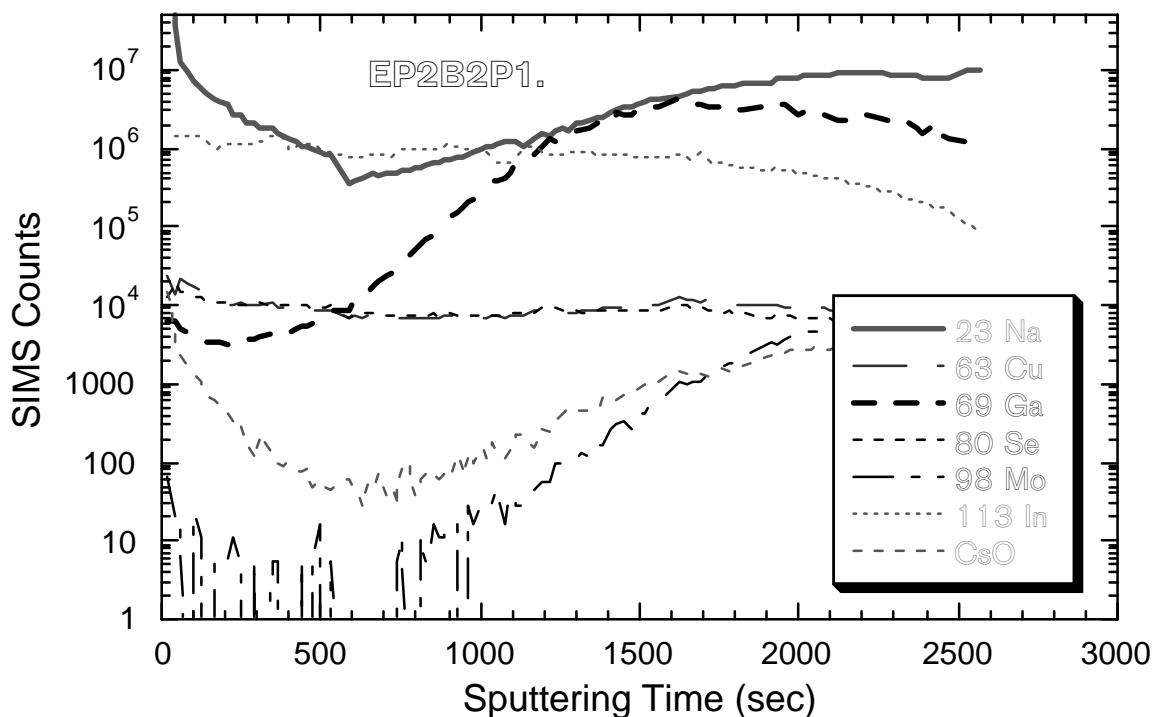


Figure 1.3. SIMS profile for EPV CIGS on Mo-coated soda-lime glass.

2.0 Zinc Oxide

2.1 Deposition and Properties

The transparent conducting ZnO applied as the final layer in the thin film coating of the module is magnetron sputtered from ceramic targets of ZnO:Al₂O₃ in a pulsed, bipolar mode. The sputtering gas is mostly argon, to which a small but carefully controlled concentration of oxygen is added. The optimal amount of oxygen is a function of deposition rate. Film properties obtained on unheated glass substrates (4300 cm² in area) are: sheet resistance 24 Ω/square, transmission 82% (for films about 0.95 μm in thickness), and conductivity 440 S cm⁻¹. The optimal thickness for use in CIGS modules is found by plotting properties on iso-efficiency contours for modules [1,3]. If ZnO of quality equivalent to that produced at EPV by RF sputtering in an R&D machine could be produced on the large substrates, then a 10% improvement in module fill factor and a 5% improvement in module current could be obtained [9]. A likely route to film improvement would seem to be substrate heating (see section 2.3 below).

Currently, a sputtering power of 1150 W is used, corresponding to a power density of 28.75 W/linear inch of racetrack. The thermal limit of these ceramic targets is not known, but

needs to be explored in order to minimize the number of ZnO cathodes used for high volume manufacturing.

2.2 Doping and Impurities

For large area zinc oxide deposition, sputtering targets containing 1.3%, 1.7% and 2% Al_2O_3 as the Al dopant source have been utilized. The zinc oxide conductivity increased from 410 S cm^{-1} to 440 S cm^{-1} after raising the Al_2O_3 concentration from 1.3% to 1.7%.

A puzzle related to unusual and inferior quality of RF sputtered ZnO was solved by replacement of the argon gas cylinder. The sheet resistance and weighted transmission of films deposited on glass using the new and old gas cylinders are shown in Figure 2.1. At a given sheet resistance, the new cylinder resulted in superior IR transmission. Impurities in the old cylinder were almost certainly to blame for the problems. It is believed that water vapor was probably the culprit.

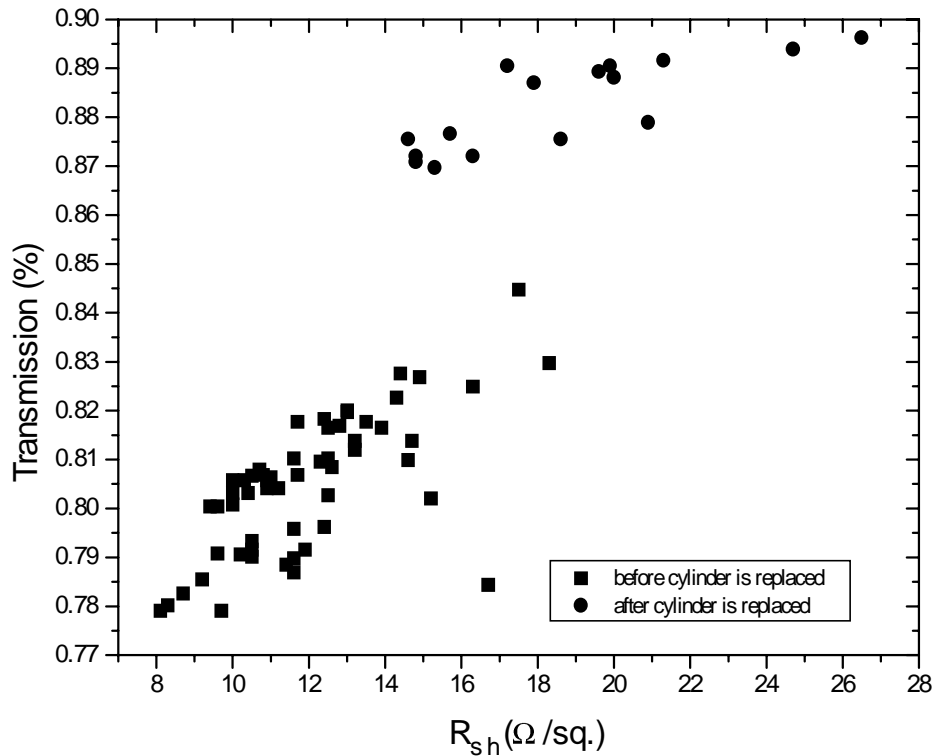


Figure 2.1. ZnO film characteristics before and after changing the Ar cylinder

2.3 Substrate Heating

Although the in-line sputtering system does not contain a substrate heater, nevertheless a suggestive result of the effect of substrate heating was obtained by pre-heating the glass substrate in an oven before insertion into the load lock. Experiments were conducted with both a single piece of glass, and a double stack for improved heat retention. Two scans were made under the cathode for each substrate, giving a film thickness of about $0.3 \mu\text{m}$. A summary of the resulting ZnO film properties is given in Table 2.1 below.

Table 2.1. Properties of ZnO prepared on unheated and pre-heated glass

Deposition	R_{sq} ohms/sq.	T_{IR} %	conductivity (ohm cm) ⁻¹
standard	86	87.6	440
pre-heated (single)	67	88.5	500
pre-heated (double)	61	89.3	529

Both conductivity and transmission of the ZnO were improved by preheating the glass. Substrate heaters have been designed for a larger in-line sputtering system recently constructed and brought into operation at EPV. It is anticipated that these heaters will be installed in the near future.

3.0 Device Studies

3.1 Baseline Process

A substantial amount of effort has been placed on achieving a reproducible process for making high efficiency CIGS in the R&D reactor by a selenization process that follows the one used in the pilot system as close as possible. Unfortunately, evolution of our standard source material makes its use in such a process undesirable, so a more reproducible way of depositing the base layer has been implemented. Very satisfactory results have been obtained with the codeposition of Ga and Se. This approach has the advantage high Ga at the Mo interface, documented in previous reports to be helpful to device fill factor and open-circuit voltage, as well as excellent reproducibility. The table below summarizes the average characteristics of 22 devices evenly distributed over the substrate surface made by this approach.

Table 3.1. Average device characteristics for the baseline selenization process.

V_{oc} (mV)	J_{sc} (mA/cm ²)	FF (%)	Eff. (%)
459	37.0	69.1	11.7

3.2 Aging and Light-soaking Effects

3.2.1 Dark aging

Longer term stability testing of devices formed by our pilot line process (or slight variations of) is underway. The vast majority of devices tested thus far suffer from “light-inhibited” degradation. Devices are stored in lab ambient between testings. A number of runs have been followed for up to 75 days at which time the samples were exposed to a one hour light-soak under approximately AM1.5 illumination in the same setup used for a-Si. After cooling, the devices were re-measured. The results of the first seven runs up to the point just before light-soaking are shown in Figure 3.1. Each run consists of about 24 devices whose characteristics are averaged. Average efficiencies range from 9-12%.

Generally, only the Voc and FF are followed as changes in Jsc have not been observed. After 75 days, efficiencies have dropped to between 83-97% of their initial value. The change observed after one week is a good indicator of the potential longer term degradation.

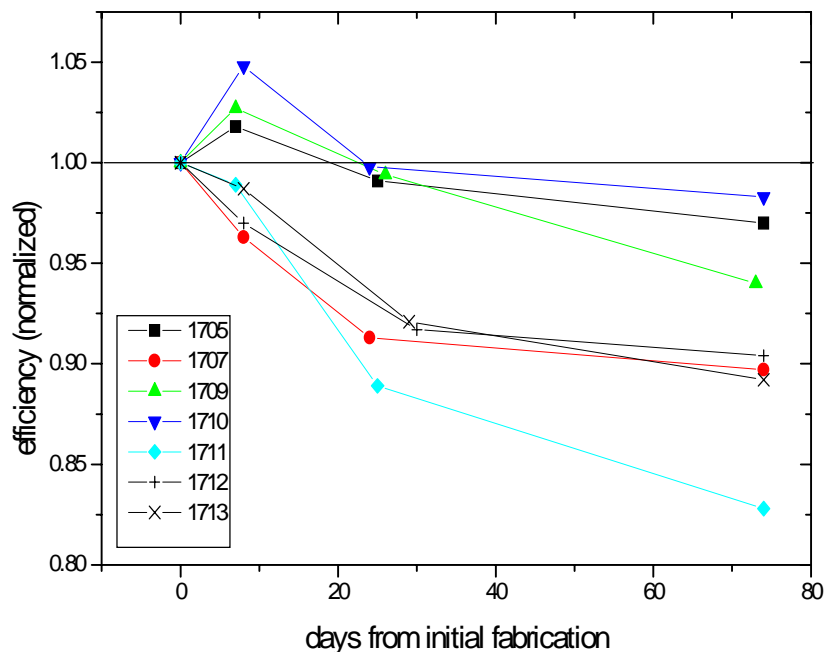


Figure 3.1. Effect of aging on average device efficiency for selenized CIGS films

Devices with intermediate initial Voc, FF products appear to degrade more than devices with greater or smaller products (Fig. 3.2), although there standard deviation for this data is quite large (not shown in the plot). It is possible that the devices with smaller products suffer from other problems that mask the effect under study.

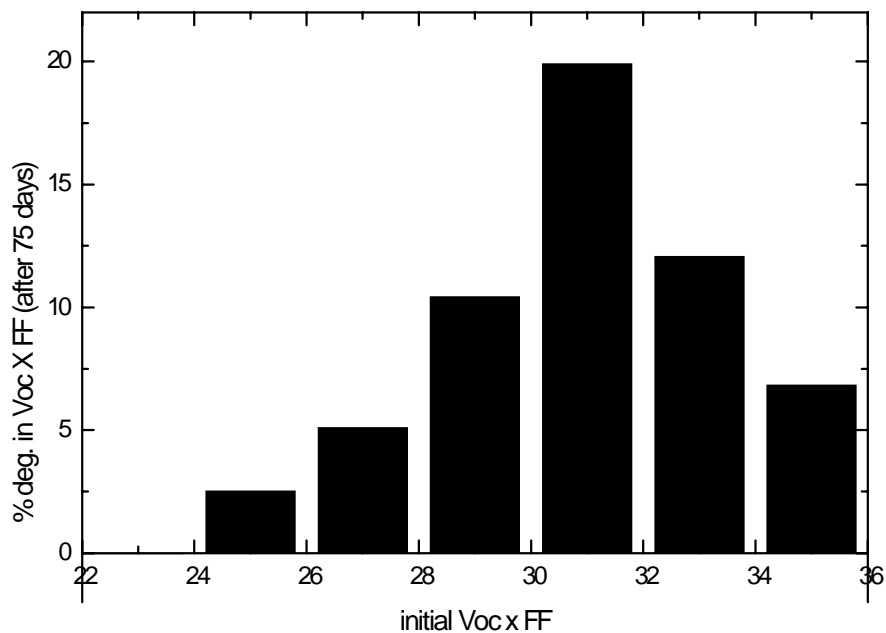


Figure 3.2. Device degradation after 75 days storage as a function of the initial $V_{oc} \times FF$.

3.22 Recovery via light soaking

The dark aging effect is reversible upon light-soaking, however the resurrection is not always complete. Table 3.2 below shows the fraction of the initial V_{oc} , FF and $V_{oc} \times FF$ the devices attained after light-soaking. Three of the seven runs achieved higher average values than those initially measured. It appears that the lower the devices fall, the more difficult it is to return them to their initial values (Fig. 3.3). In the case of run 1711, no significant difference in characteristics was observed between 1 hour and 40 hours of light-soaking. This implies that the degradation is occasionally irreversible. For devices that do not return to their original efficiency after light-soaking, the cause is almost always due to a lower V_{oc} . In almost all cases, these devices are the closest to being Cu-rich.

Table 3.2. Ratios of V_{oc} , FF, and $V_{oc} \times FF$ after 1 hr. light-soaking at AM1.5 relative to their initial values.

run #	V_{oc}	FF	$(V_{oc} \times FF)$
1705	1.005	1.009	1.014
1707	0.988	0.969	0.959
1709	1.003	1.016	1.020
1710	1.018	1.029	1.048
1711	0.949	0.987	0.937
1712	0.974	0.986	0.960
1713	0.969	0.994	0.964

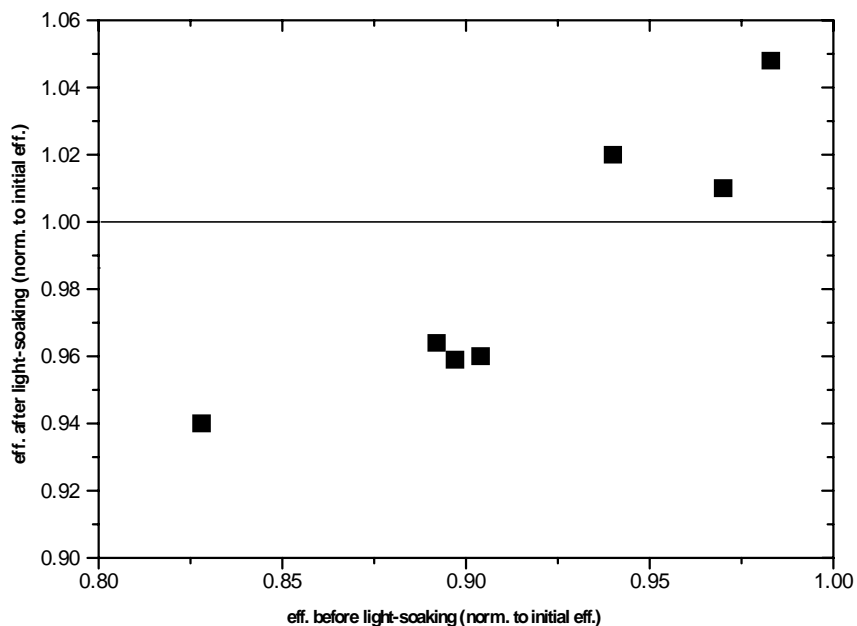


Figure 3.3. Average efficiency of runs after 1 hr. light-soaking vs. the average efficiency prior to light-soaking, both normalized to the initial efficiency.

To gain further insight into the light-soaking effects observed in devices made from selenized CIGS, diode parameters have been extracted by modeling the J-V characteristics as a function of light-soaking time. Device 1705a1 was measured several times at 100 mW/cm² while being light-soaked between 3 - 3455 seconds under short-circuit conditions. 3 seconds was the amount of time during the initial measurement for the I-V region of interest to be measured. The sample was heat-sunk to an Al block with a silicone heat sink compound during the measurements. As previously observed, the fill factor increased with increasing light-exposure. The standard device characteristics for each light-exposure time are listed in Table 3.3 below, with some of the curves being shown in Figure 3.4 following.

Table 3.3. Device parameters as a function of light-soaking time.

soak time (s)	V _{oc} (V)	I _{sc} (mA)	FF (%)
1	0.483	5.34	58.6
5	0.481	5.43	60.2
40	0.480	5.44	62.5
155	0.472	5.36	64.3
455	0.479	5.45	65.6
1055	0.473	5.51	64.7
3455	0.476	5.67	65.9

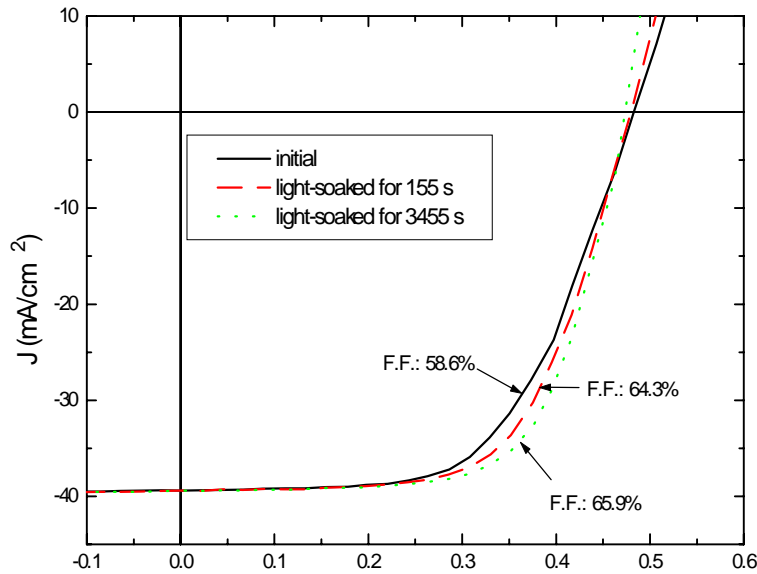


Figure 3.4. J-V characteristics as a function of light-soaking time.

The I-V data were modeled and the series resistance and diode quality factor were extracted using the method of Sites and Mauk [10]. The results for these two parameters are plotted below as a function of the light exposure time. The series resistance was observed to drop from about 2.6 to 1.0 Ωcm^2 . The decrease in series resistance was nearly linear when plotted on a semi-log scale. The experimental diode quality factor, on the

other hand, remained nearly constant within experimental error over the measurement interval.

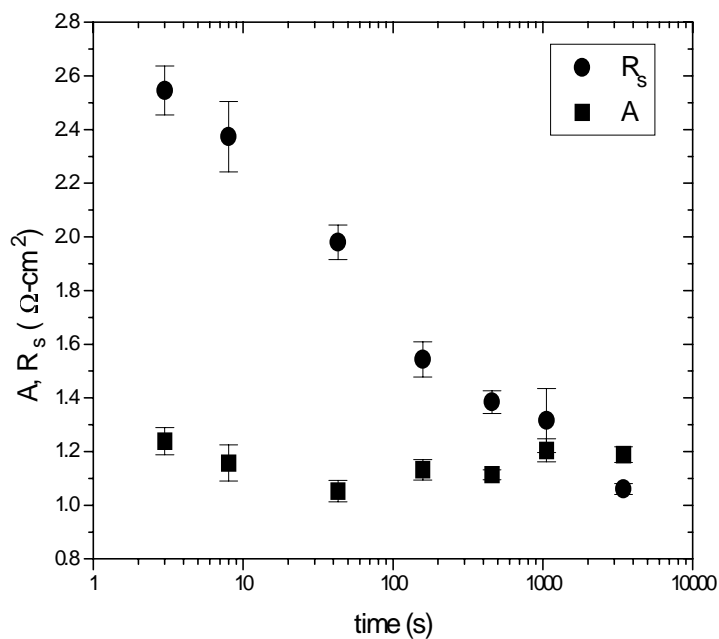


Figure 3.5. Experimental diode quality factor and series resistance as a function of light-soaking time.

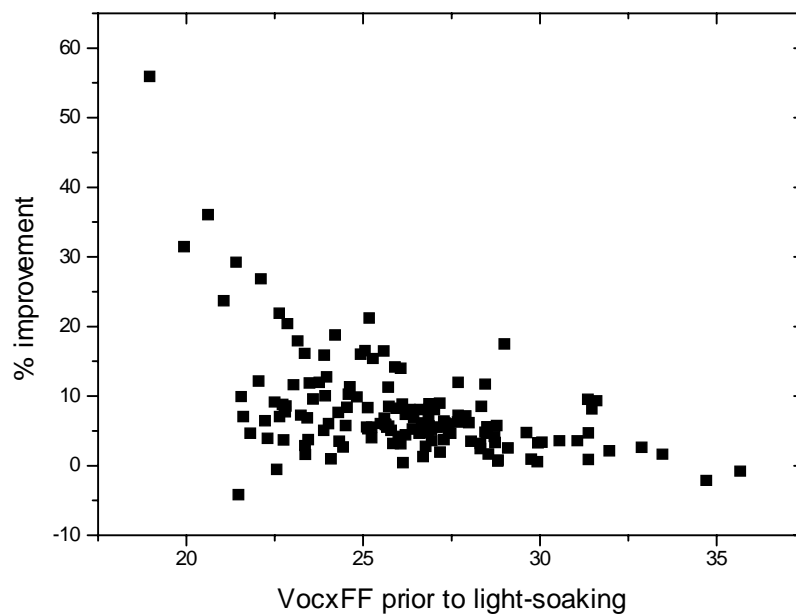


Figure 3.6. The improvement of devices upon light-soaking as a function of their V_{oc} , FF product prior to light-soaking.

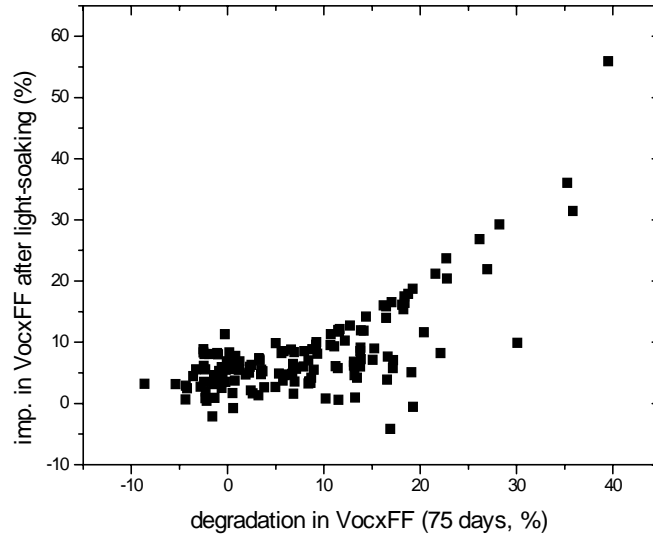


Figure 3.7. The improvement of devices upon 1 hr. light-soaking as a function of the amount of degradation in the V_{oc} , FF product after 75 days.

3.23 Cyclic dark aging/light soaking

Further analysis of the light-soaking effect has revealed that, not surprisingly, the effect is somewhat reversible. The data for one set of contacts (24) from one run (H1725) is shown in Figure 3.8 below. The data is normalized to the initial efficiency and averaged. So that the effect could be explored in a short time frame, the cells were made with an especially thin CdS layer which apparently accelerates the degradation. The cells were measured, light-soaked for one hour, and then re-measured at periods of 8, 29, 36, and 57 days. The cells returned nearly to their original efficiency after each light-soaking. What is surprising is that the degree of degradation diminishes after several light-soakings. It is unknown whether the effect is due to the accumulated light exposure (like charging a battery), the cycling between illuminated and unilluminated states, or simple aging. These samples will be followed to further explore this effect. Meanwhile, experiments will be conducted to explore the other hypotheses.

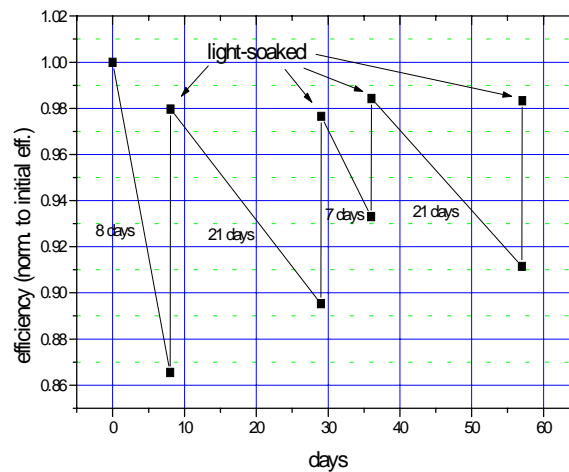


Figure 3.8. Normalized efficiency of devices from H1725 over the course of time.

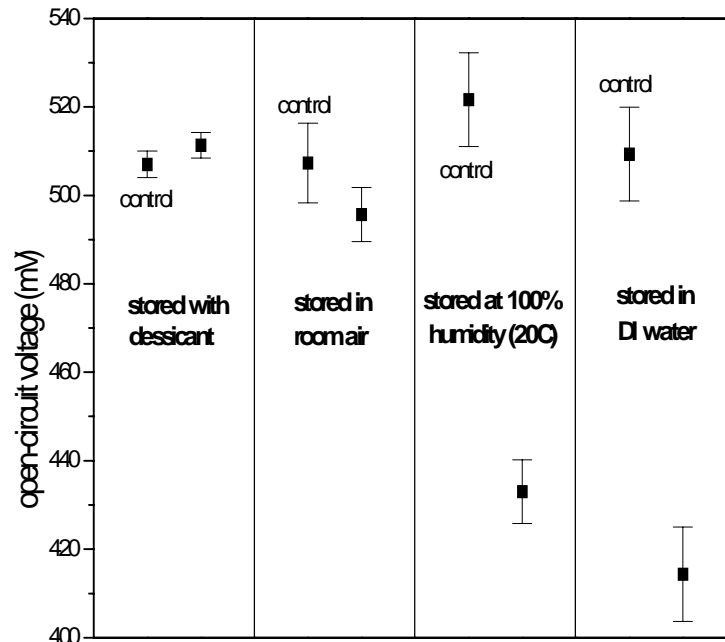
Other process parameters that influence the light-inhibited degradation besides the Cu/In ratio (Se flux, temperatures, termination, CdS thickness, etc.) are being examined. In this regard, cells near the center of the sample area are generally of higher quality than those around the perimeter. Another parameter with some apparent control over the change in $V_{oc} \times FF$ after a one week period is the CdS thickness. One possibility is that a thicker CdS film leads to a higher roomlight V_{oc} (this is fact) sufficient to effect a degree of light-soaking.

3.24 Effect of moisture after CIGS formation

The effect of moisture between the formation of CIGS and further window layer processing has been explored. CIGS was formed by selenizing and terminating a pilot line precursor in the R&D reactor. The CIGS was cut into pieces and stored for 15 hours under various conditions before CBD CdS and ZnO were deposited. The four conditions were:

- 1) stored with desiccant in a sealed container
- 2) stored in room air
- 3) stored at 100% humidity at 20°C in a sealed container
- 4) stored in DI water at room temperature

An adjacent piece of each sample was stored in vacuum during this interval as a control and all pieces were processed together for CdS and ZnO. Devices were made and tested the same day. The results are shown in Figure 3.9. There was no discernible degradation observed for the sample stored in desiccant. The other 3 samples showed significant degradation in the order: room air, 100% humidity, DI water. It may be concluded that the primary cause of degradation of the devices is related to moisture, not oxygen alone, and is probably associated with the diffusion of sodium from the glass.



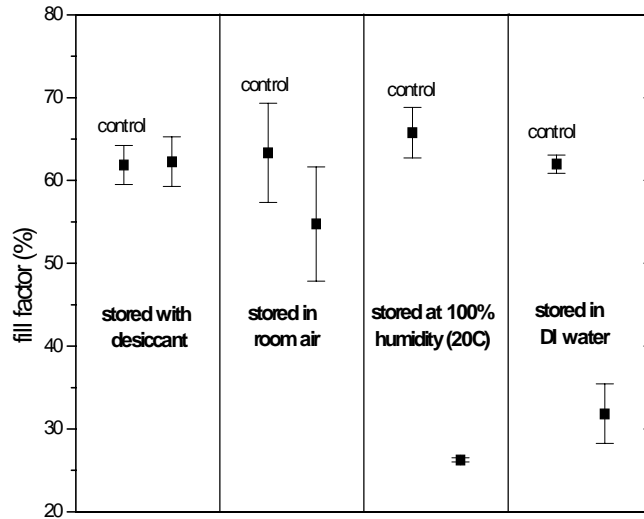


Figure 3.9. Effect of CIGS storage under various conditions prior to CdS/ZnO deposition.

3.25 Stability of CIGS prepared by the new FORNAX process

Three sets of devices from runs H1751, H1754, and H1761 have been tracked to determine the stability of device characteristics. All three CIGS depositions were made by the FORNAX technique and window layers were deposited in the standard fashion (CBD CdS, sputtered ZnO). Average total area device efficiencies for all three sets were 10-11%. Each data point in Figure 3.10 represents the average of 24 devices or slightly fewer (some were damaged during testing), normalized to their initial $V_{oc} \times FF$. No intentional light-soaking was employed. Samples were stored in lab ambient between measurements. Thus far, all three device sets have changed less than 2% in $V_{oc} \times FF$ during the course of this study, probably well within the measurement error. Most devices made from selenized CIGS had degraded considerably more during a similar period stored in the same location (up to 13%). This monitoring will be continued to more fully verify the device stability.

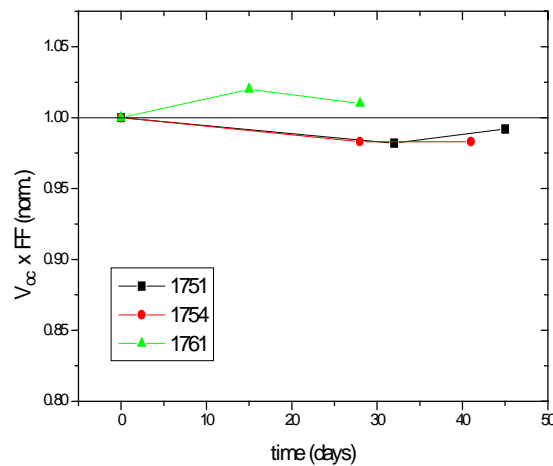


Figure 3.10. Change in $V_{oc} \times FF$ for three sets of FORNAX devices as a function of time. Devices were stored in lab ambient between measurements.

4.0 Minimodule Fabrication

4.1 Purpose and Methods

To qualify the CIGS process for module manufacture, and to determine the module efficiency that can be expected if all films were uniform, minimodules are fabricated. Laser scribing was used for the Mo (see section 5.3), while the 2nd and 3rd scribes (P2 and P3) were performed mechanically on a small x-y table. Modifications were made to the mechanical scribing of P2 to expose a wider area by making two scribes offset by 50 μm . The total width of P2 is now about 150 μm . This action was taken based on evidence that series resistance is introduced if the width of P2 is too narrow ($< \sim 60 \mu\text{m}$).

4.2 Results

Four test interconnects were made from the CIGS samples of run 1724. The I-V characteristics of the four interconnects are shown in the I-V plot (Figure 4.1) and table (Table 4.1) below.

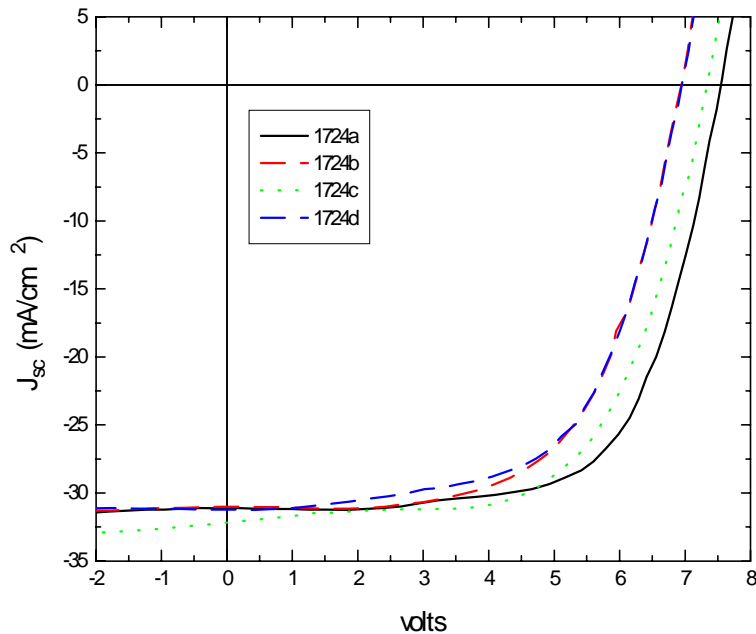


Figure 4.1. I-V curves of a set of minimodules from run 1724.

Table 4.1. Photovoltaic parameters of the set of minimodules.

sample	area cm^2	cells	Voc volts	Isc mA	FF %	P_{max} W	Eff. %
1724a	32.8	16	7.55	63.8	66.0	0.318	9.7
1724b	33.0	15	6.94	68.1	62.1	0.293	8.9
1724c	33.6	16	7.33	67.6	61.9	0.307	9.1
1724d	33.0	15	6.95	68.7	61.2	0.292	8.9

Samples 1724b and 1724d were less Cu-poor (and close to Cu-rich at one end) than the other two samples and have slightly lower V_{oc} 's as a result. The higher fill factor of 1724a is at least partly due to higher quality CIGS, but may also be a result of an accident during ZnO deposition (one end of the sample slipped from the mounting plate during deposition and became very hot). The sheet resistance of ZnO films deposited on glass under the same conditions was 10-12 Ω /sq. Because the sheet resistance of ZnO deposited on CIGS/CdS is typically 20-30% higher, the sheet resistance of ZnO on the interconnects is probably 12-16 Ω /sq. The effective total area J_{sc} on all four samples is 31 - 32 mA/cm² while the J_{sc} on test devices made in identical runs (with R_{sh} of 16-18 Ω /sq.) is 37 -38 mA/cm². Allowing for a 10% interconnect area loss, 2-3 mA/cm² remain to be accounted for. At least some of this loss may be due to absorption in the slightly thicker ZnO. It was later discovered that the sputtering gas contained impurities (probably water) that degraded the optical qualities of the ZnO. This problem was eliminated by replacing the gas cylinder. An aperture area efficiency of 9.7% was achieved in this series of samples.

5.0 Module Fabrication and Performance

5.1 Processing Steps

The major processing steps involved in module fabrication are listed in Table 5.1. Some of these steps consist of several distinct operations. For example, precursor deposition involves multiple depositions of different materials (by sputtering and linear source evaporation), and preparation for lamination involves edge isolation, bus bar attachment, hole drilling for lead out, and layout of the EVA film. Also shown in this table are quality control procedures and characterization methods applicable to each step.

Table 5.1 *Quality Control Procedures for CIGS Module Fabrication*

Operation	QC/Characterization
1. Select glass	Determine tin side
2. Wash glass	Inspection
3. Sputter Mo	Contactless sheet resistance; thickness; mechanical stress
4. Laser scribe (P1)	Check isolation
5. Deposit precursor	Thickness; mass
6. CIGS compound formation	Resistance; composition; thickness
7. CBD CdS	Color; transmission
8. Sputter initial ZnO	Sheet resistance; diagnostic V_{oc} , I_{sc}
9. Mechanical scribe (P2)	Exposure of Mo
10. Sputter final ZnO	Sheet resistance; thickness; transmission
11. Mechanical scribe (P3)	Module I-V; diagnostic cell I-V; QE; thermal imaging; contact res.
12. Prepare for lamination	Inspection
13. Vacuum laminate	Module I-V; inspection
14. Attach boot and wires	Inspection
15. Cure	Module I-V; label

5.2 Linear Source Evaporation

The ability of appropriate linear source designs to deposit a substantially uniform thin film across a substrate moving in a direction perpendicular to the axis of the source has been verified by modeling [1]. For each full pass of the substrate under a source with constant emission strength, the relative thickness distribution in the x direction (x parallel to the source, and the source extending from x_1 to x_2) is

$$t(x) \propto (x_2 - x)/\sqrt{h^2 + (x_2 - x)^2} - (x_1 - x)/\sqrt{h^2 + (x_1 - x)^2}$$

where h is the height of the source above the substrate. In Figure 5.1 we show the thickness distribution obtained for a simple 20" source spaced at 2,3,4,5, and 6" from the substrate, and the distribution obtained for an optimized source at an appropriate spacing. For the latter 20" source a uniform coating width of about 16" can be obtained. Scaling to longer sources is straightforward.

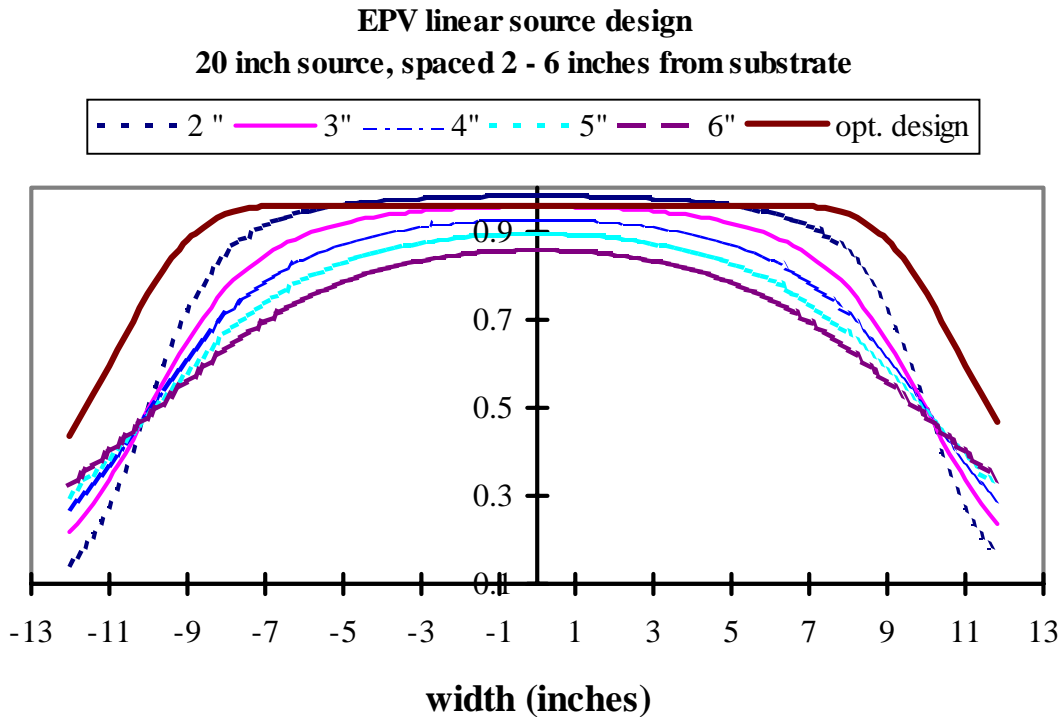


Figure 5.1. Thickness profiles obtained for simple and optimized linear evaporation sources

5.3 Patterning

The function of the first patterning step is to separate the Mo into isolated strips. This step can be accomplished by laser scribing using the green beam (532 nm) of a frequency-doubled YAG laser. The Mo-coated plate is mounted on an x-y table and translated under the stationary laser beam. The controlling software is written by EPV. Currently, a fiber coupled, laser diode pumped, Q-switched laser operating in TEM₀₀ mode is employed. An

LBO crystal is used for doubling, and an acousto-optic Pockels cell for Q-switching. Verification of electrical isolation between the Mo strips is performed as part of quality control.

The second and third patterning steps are performed to expose the Mo and to sever the ZnO. These steps can be accomplished by mechanical scribing of the CIGS using a blade shape chosen to minimize the width of the cut. During Phase III, various upgrades were made to the system so that the scribing operation is now semi-automated. These upgrades included addition of a computer system and user-interface software, closed-loop servo motor indexing of position, and addition of safety limit switches for over travel protection. The improvements allow for more accurate positioning of the knives ($\approx 10\mu\text{m}/\text{step}$), higher throughput, and better plate-plate repeatability.

5.4 Encapsulation

Preparation of the patterned CIGS plate for lamination includes removal of films around the periphery of the substrate, attachment of Al foil bus bars by ultrasonic welding, and drilling of the substrate for lead out. The interconnect scheme and foil location is shown in Figure 5.2.

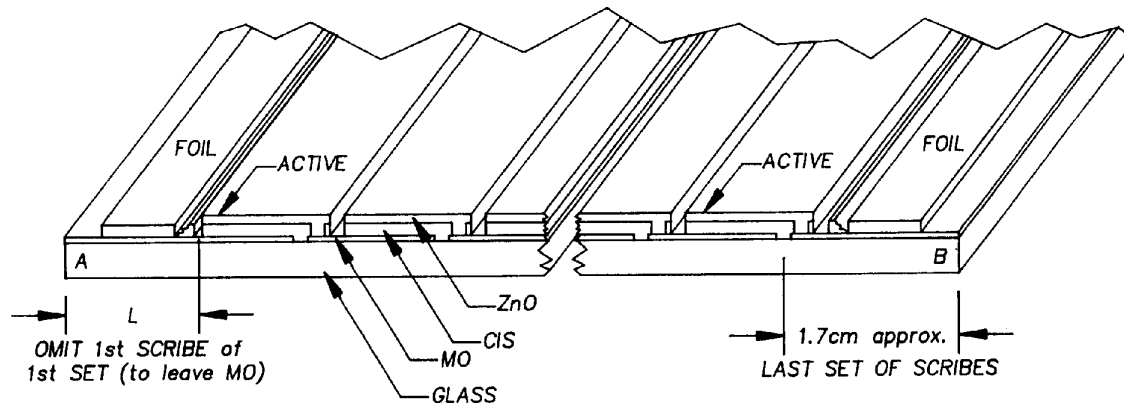


Figure 5.2. Monolithically integrated CIGS module showing interconnect scheme and metal foil busbars at module edges.

The layout of the monolithically-interconnected plate prior to lamination is shown in Figure 5.3. The standard plate area is 4294 cm^2 . Lamination is performed in a vacuum laminator using fast cure EVA in sheet form. Electrical connections to the module are made via two strain-relieved, insulated wires that are connected to the foils under a silicone boot for environmental protection. The module is frameless, and is mounted via four Al extrusions glued to the back of the substrate glass. This encapsulation scheme is similar to the one used by EPV in its fabrication of tandem junction a-Si modules.

Layout of CIGS Plate before Encapsulation

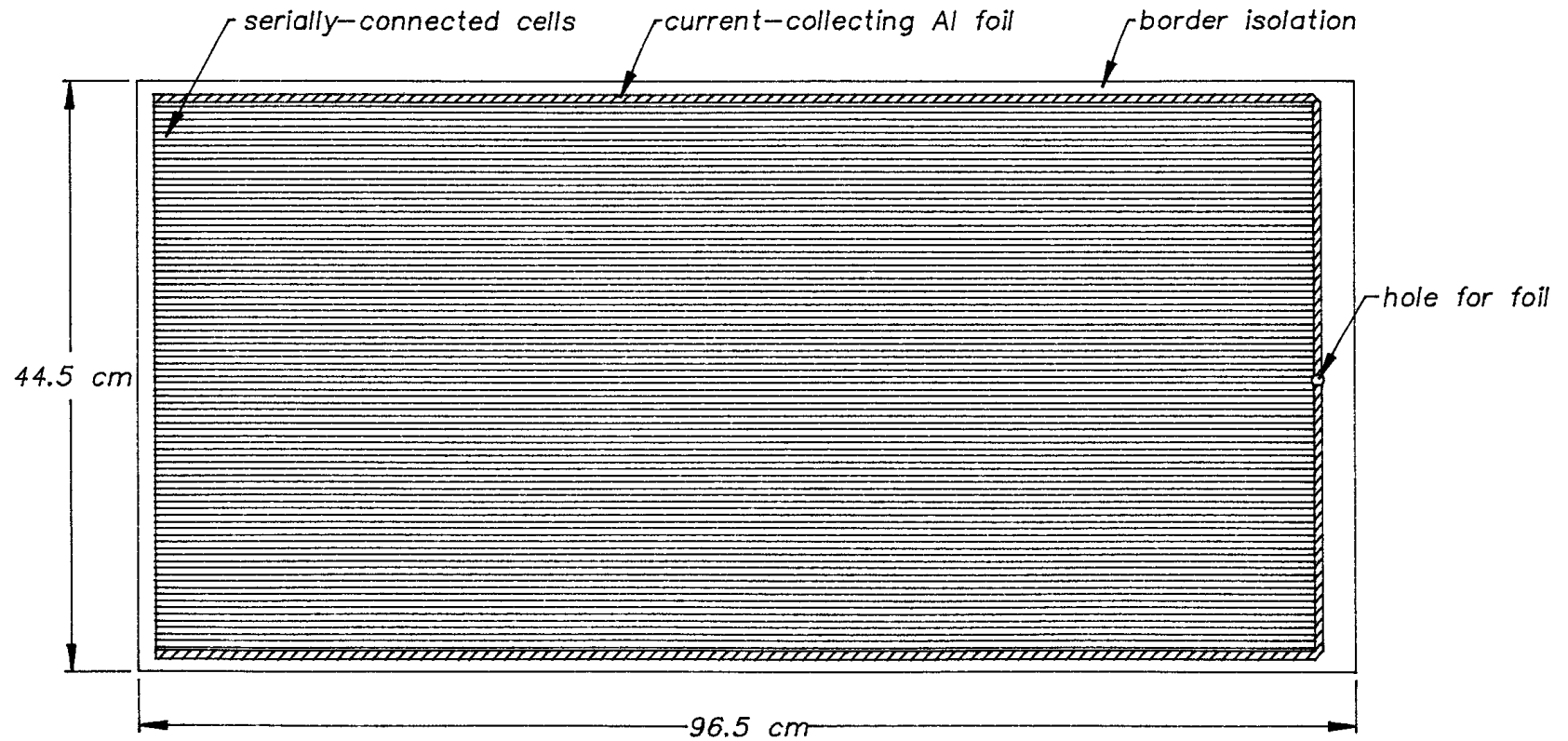
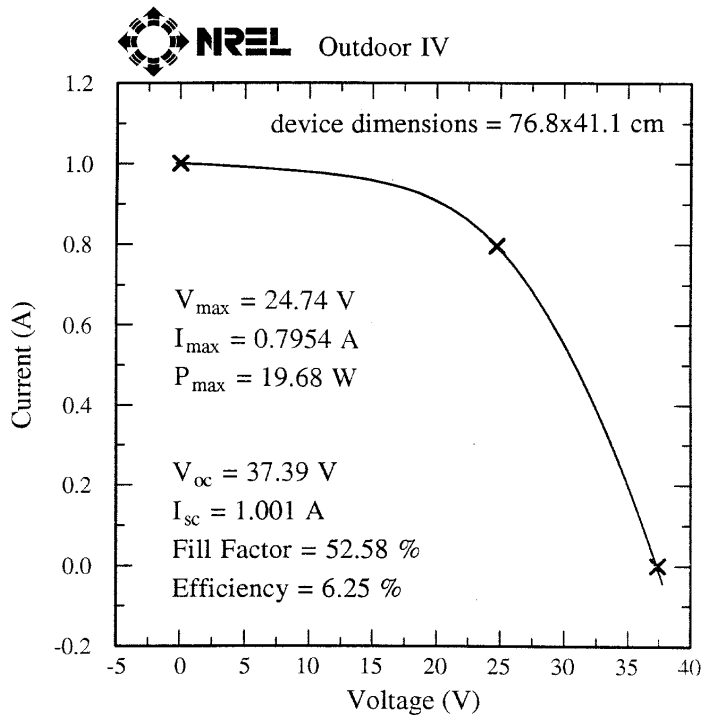


Figure 5.3. Layout of CIGS plate prior to lamination.

5.5 Module Performance

After completion of full-size plates in the pilot line, diagnostic testing usually reveals one or two edge regions to have somewhat inferior performance. Occasionally an edge region is cut off, and the resulting plate is then re-tested and laminated. One such plate was laminated with EVA to a low-iron cover glass and sent to NREL for efficiency verification. The NREL I-V curve for this module, obtained in sunlight, is shown in Figure 5.4. The aperture area of this module was 3156 cm², and the corresponding efficiency 6.25%. The module produced 19.7 watts at 997 W/cm² irradiance and a module temperature of 24.9 °C, the PV parameters being $V_{oc} = 37.4$ V (average V_{oc} per cell 456 mV), $I_{sc} = 1.00$ A, and $FF = 52.6\%$.

Sample: Z740B	area used = 3156.5 cm ²
Apr 3, 1997 1:53 PM MST	997.2W/m ² fixed tilt
device Temperature = 24.9°C	Si Ref. cell #294278



Air temperature = 18.1°C, Air mass = 1.35, POA sun angle = 27.4°
total irradiance from K&Z CM11 = 999.2 W/m²

Figure 5.4. I-V curve measured by NREL for a 19.7 watt, 3156 cm² glass-glass encapsulated CIGS module.

A later plate, measured in sunlight at EPV, produced 25.0 watts at an irradiance of 1052 W/cm², corresponding to an aperture area (3100 cm²) efficiency of 7.65%. The PV parameters were $V_{oc} = 31.0$ V, $I_{sc} = 1.46$ A, and $FF = 55.4\%$. The I-V curve is shown in Figure 5.5.

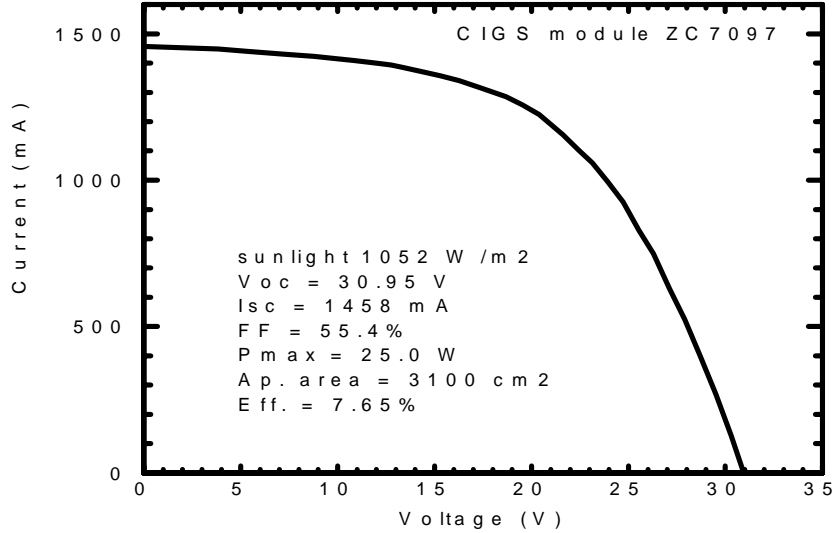


Figure 5.5. I-V curve measured in sunlight at EPV for a 25 watt, 7.65% CIGS module.

5.6 Module Diagnostics

A new diagnostic technique was developed at EPV in order to be able to map the quality of the CIGS device across a large monolithic plate in a non-destructive manner [1-3]. The method is illustrated in Figure 5.6. The entire module is illuminated and driven through its I-V curve by a computer-controlled bipolar supply, while three probes pick up voltages from which *local* cell current and voltage values can be inferred. The positioning of the probes is shown in the inset to the figure. The intrinsic I-V curve of the cell on which the 2nd and 3rd probes are placed is obtained by plotting $V_{23} = V_2 - V_3$ (proportional to cell current) versus $V_{12} = V_1 - V_2$ (cell voltage). The fill factor of the cell is then calculated in the usual way. Prior to invention of this technique, determination of the fill factor at a given location on a plate required destructive scribing of the films to isolate a small diagnostic cell. If, as a reasonable first approximation, it is assumed that the module short-circuit current distributes evenly across the plate, then the local sheet resistance of the zinc oxide can be calculated from the measured V_{23} as $R_{sq} = 2V_{23} / [J_{sc}(x_3^2 - x_2^2)]$, where x_3 and x_2 are the distances of probes 3 and 2 from the edge of the cell.

The technique has been used to map Voc and FF across the surface of large area, patterned CIGS plates and has been instrumental in detecting gradients in performance [2]. The technique has also been applied to decompose the measured fill factor of a CIGS module into the intrinsic device fill factor and the effect of ZnO sheet resistance. Existing diagnostic data concerning the local device fill factor for seven CIGS modules were averaged across each plate (see Table 5.2). Next, from computer modeling of module fill factor (at 1000 W/m²) versus ZnO sheet resistance, fill factor reduction factors (defined as $FF(R_{sq}) / FF(R_{sq} = 0)$, where R_{sq} is the ZnO sheet resistance) were calculated. The predicted module fill factor was then calculated as diagnostic fill factor times fill factor reduction factor. From Table 5.2 it can be seen that this calculation, using the average

diagnostic fill factor and diagnostic ZnO sheet resistance determined by the new techniques, indeed closely predicted the actual measured module fill factor. This confirms our ability to quantify the relative contributions of intrinsic device fill factor and ZnO sheet resistance in determining the fill factor of a module. This understanding is an important tool for further module optimization.

Table 5.2. Comparison of predicted module fill factor (based on diagnostic data) and measured module fill factor for seven CIGS modules

Average diagnostic FF (%)	diagnostic ZnO Rsq (ohms/sq.)	FF reduction factor	predicted module FF (%)	measured module FF (%)
62.0	27	0.83	51.4	54.5
63.5	36	0.77	49.0	50.8
58.0	30	0.81	47.2	46.6
57.3	38	0.76	43.8	46.5
60.8	51	0.70	42.6	41.9
50.2	33	0.79	39.8	40.4
43.4	54	0.68	29.4	31.1

References

1. Delahoy, A.E. and Meyers, P.V., "Thin-Film PV Modules: Manufacturing Technology and Issues," Tutorial III, 26th IEEE Photovoltaic Specialists Conference, September 29, 1997.
2. Britt, J.S., Delahoy, A.E., and Kiss, Z.J., "Pilot Production of CIGS Photovoltaic Modules," *Proceedings of the 26th IEEE Photovoltaic Specialists Conference*, Anaheim (IEEE, 1997) pp. 335-338.
3. Britt, J.S., Delahoy, A.E., and Kiss, Z.J., "Large Area Coating of CIGS and ZnO for Photovoltaics," *Proceedings of the 14th European Photovoltaic Solar Energy Conference*, Barcelona (H.S. Stephens, 1997) pp. 1287-1290.
4. Noufi, R., Axton, R., Herrinton, C., and Deb, S., *Appl. Phys. Lett.* **45** (1984), 668.
5. Kohara, N., Negami, T., Nishitani, M., and Wada, T., *Jpn. J. Appl. Phys.* **34**, 2 (1995) L1141.
6. Zwiegart, S., Schock, H.W., and Powalla, M., *Proceedings of the 14th European Photovoltaic Solar Energy Conference*, Barcelona, Spain, (H.S. Stephens, 1997) pp.1254-1257.
7. Yamanaka, S., McCandless, B. E., Birkmire, R. W., *Proceedings of the 23rd IEEE Photovoltaic Specialists Conference*, 1993, 607.
8. Marudachalam, M., Birkmire, R., Schultz, J., and Yokimcus, T., *1st World Conference on Photovoltaic Energy Conversion* (1994) 234.
9. Delahoy, A.E., Britt, J.S., Kiss, Z.J. (1997) "CIS Photovoltaic Technology." *Annual Technical Progress Report, NREL/SR-520-23194*. 38pp. Available NTIS: Order No. DE 97050822.
10. Sites, J.R., and Mauk, P.H., *Solar Cells*, **27** (1989) 411-417.

REPORT DOCUMENTATION PAGE			Form Approved OMB NO. 0704-0188	
Public reporting burden for this collection of information is estimated to average 1 hour per response, including the time for reviewing instructions, searching existing data sources, gathering and maintaining the data needed, and completing and reviewing the collection of information. Send comments regarding this burden estimate or any other aspect of this collection of information, including suggestions for reducing this burden, to Washington Headquarters Services, Directorate for Information Operations and Reports, 1215 Jefferson Davis Highway, Suite 1204, Arlington, VA 22202-4302, and to the Office of Management and Budget, Paperwork Reduction Project (0704-0188), Washington, DC 20503.				
1. AGENCY USE ONLY (Leave blank)	2. REPORT DATE October 1998	3. REPORT TYPE AND DATES COVERED Final Technical Report		
4. TITLE AND SUBTITLE CIS Photovoltaic Technology; Final Technical Report			5. FUNDING NUMBERS C: ZAF-5-14142-04 TA: PV905001	
6. AUTHOR(S) A.E. Delahoy, J.S. Britt, and Z.J. Kiss				
7. PERFORMING ORGANIZATION NAME(S) AND ADDRESS(ES) Energy Photovoltaics, Inc. 276 Bakers Basin Road Lawrenceville, NJ 08648			8. PERFORMING ORGANIZATION REPORT NUMBER	
9. SPONSORING/MONITORING AGENCY NAME(S) AND ADDRESS(ES) National Renewable Energy Laboratory 1617 Cole Blvd. Golden, CO 80401-3393			10. SPONSORING/MONITORING AGENCY REPORT NUMBER SR-520-25713	
11. SUPPLEMENTARY NOTES NREL Technical Monitor: H.S. Ullal				
12a. DISTRIBUTION/AVAILABILITY STATEMENT National Technical Information Service U.S. Department of Commerce 5285 Port Royal Road Springfield, VA 22161			12b. DISTRIBUTION CODE	
13. ABSTRACT (<i>Maximum 200 words</i>) This report describes work performed by Energy Photovoltaics, Inc. (EPV) during the third phase of a three-phase, cost-shared subcontract. Researchers at EPV explored novel sequential formation recipes for CIGS that can be implemented on a unique pilot line constructed to coat low-cost, glass substrates 4300 cm ² in area; implemented a particular CIGS recipe on the pilot line that enabled large-area modules to be prepared with efficiencies up to 7.6%; and performed electrical resistance monitoring of the film that proved capable of indicating the temperature of compound formation and detecting termination. The substrate/Mo/Na working group (which included EPV, NREL, and others) studied Na in Mo and the effect of Na on devices, and found it beneficial except at concentrations exceeding 0.4%. Researchers determined the following properties of large-area, magnetron-sputtered ZnO:Al: sheet resistance 24 Ω/sq., transmission 82%, conductivity 440 S cm ⁻¹ ; and preheating the glass increases the conductivity. Devices prepared using a baseline CIGS process averaged 11.7% in efficiency. Modules and minimodules were prepared using a diode-laser-pumped yttrium-aluminum-garnet laser for the Mo patterning and mechanical scribing for the cuts. Large-area CIGS formation involves the use of linear sources, and thickness profiles were presented for simple and optimized linear sources. An unencapsulated module producing 25 watts (7.65% aperture-area efficiency) was produced. Using a new diagnostic technique, the fill factor of a CIGS module was decomposed into contributions from the intrinsic device fill factor and ZnO sheet resistance.				
14. SUBJECT TERMS photovoltaics ; Thin Film PV Partnership Program ; Cu(In,Ga)Se ₂ ; CIGS ; module fabrication ; module performance ; sodium			15. NUMBER OF PAGES 39	
			16. PRICE CODE	
17. SECURITY CLASSIFICATION OF REPORT Unclassified	18. SECURITY CLASSIFICATION OF THIS PAGE Unclassified	19. SECURITY CLASSIFICATION OF ABSTRACT Unclassified	20. LIMITATION OF ABSTRACT UL	